JACS
JOURNAL OF THE AMERICAN CHEMICAL SOCIETY
pubs.acs.org/JACS
Article

Insights into the Wastewater-Free Synthesis of Zeolites

Lifan Deng,[▽] Caiyi Lou,[▽] Qinming Wu,* Xiaolong Liu, Jing Niu, Xiaohui Du, Shutao Xu,* Liang Wang, Zhongmin Liu, Jihong Yu,* and Feng-Shou Xiao*

Cite This: J. Am. Chem. Soc. 2025, 147, 42901−42908
Read Online
ACCESS | Metrics & More | Article Recommendations | Supporting Information

ABSTRACT: Conventional synthesis of zeolites produces a large amount of alkaline wastewater containing organic substances and dissolved silica species from hydrothermal crystallization, washing, and ion-exchange procedures, which are environmentally unfriendly and costly. To avoid these drawbacks, a near-neutral and solvent-free synthetic route has been developed, which simplifies the zeolite synthesis and post-treatment procedures, containing only grinding, crystallization, and calcination, achieving zero emission of wastewater. Furthermore, the reactor in this process has been scaled up to 300 L, which is an industrial scale for zeolite synthesis. Because of the solvent-free and near-neutral conditions, *ex situ* ^{29}Si MAS NMR and *in situ* ^{29}Si, ^{13}C, and ^{1}H MAS NMR were successfully employed for the characterization of zeolite crystallization, showing that the silica species basically remain as a large amount of Si(4Si) species during zeolite crystallization, a typical feature of the solid-state phase transformation mechanism. Furthermore, 2D ^{1}H−^{29}Si HETCOR MAS NMR analyses reveal the interaction between Si(4Si) species in the zeolite framework and the methyl and methylene groups of the TPA^{+} template, suggesting a potential templating contribution. This work not only presents an environmentally friendly strategy suitable for industrial-scale zeolite production but also offers fundamental insights into the solid-state phase transformation mechanism.

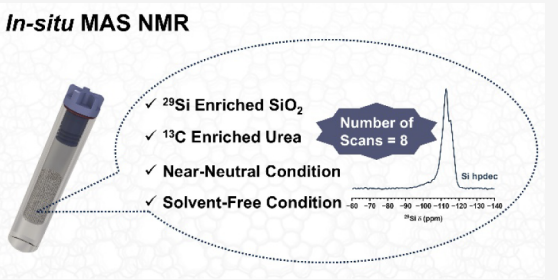

INTRODUCTION

Zeolites have been widely utilized in petroleum refining, petrochemical industries, and chemical industries owing to their superior characteristics.[1−6] However, the crystallization and treatment processes of zeolites normally produce large amounts of alkaline wastewater containing dissolved silica and organic templates, requiring neutralization, deamination, and the removal of organic templates during the production of zeolites, which is environmentally unfriendly and costly.[7−9]

To address these challenges, Xu et al. developed a dry gel conversion (DGC) method for the synthesis of zeolites.[10] Nevertheless, the preparation of dry gels still relied on hydrothermal conditions, followed by solvent vaporization, mixing of raw materials, and crystallization, leading to low space−time yields. Xiao et al. reported a solvent-free route for the synthesis of zeolites, in which silica, an aluminum source, alkali, and an organic template were directly mixed and crystallized. Because inorganic alkali was added in the starting materials, it was necessary to remove these inorganic cations by ion-exchange and washing procedures, thus the formation of a large amount of wastewater was inevitable.[11,12] Recently, Xiao et al. reported a near-neutral synthesis of zeolites, where urea decomposed to produce NH_3 and CO_2. The NH_3 dissolved in water to form $NH_3{\cdot}H_2O$, thereby providing the necessary OH^- for the depolymerization and condensation of the silica source during zeolite crystallization. In this process, the alkali was free, and the ion-exchange step was not necessary.[13] However, there is still the formation of wastewater due to hydrothermal conditions.

To fully avoid the formation of wastewater, a combination of solvent-free with near-neutral synthesis is proposed, which should not only be wastewater-free but also simplify the synthetic steps to only mixing, crystallization, and calcination. This simple process is highly favorable for the industrial production of zeolites.

Recently, there have been great successes in the characterization of aluminophosphate-based molecular sieves by ^{27}Al and ^{31}P MAS NMR under near-neutral conditions,[14−17] but it is still difficult to perform *in situ* MAS NMR characterization of silica-based zeolite crystallization due to the complexity in the presence of solvent and alkali, as well as the low natural abundance of ^{29}Si species. In this work, by combining solvent-free with near-neutral conditions and the use of isotopically labeled $^{29}SiO_2$,[18−20] it is possible to gain insights into silica-based zeolite crystallization.

Received: September 6, 2025
Revised: October 28, 2025
Accepted: October 29, 2025
Published: November 6, 2025

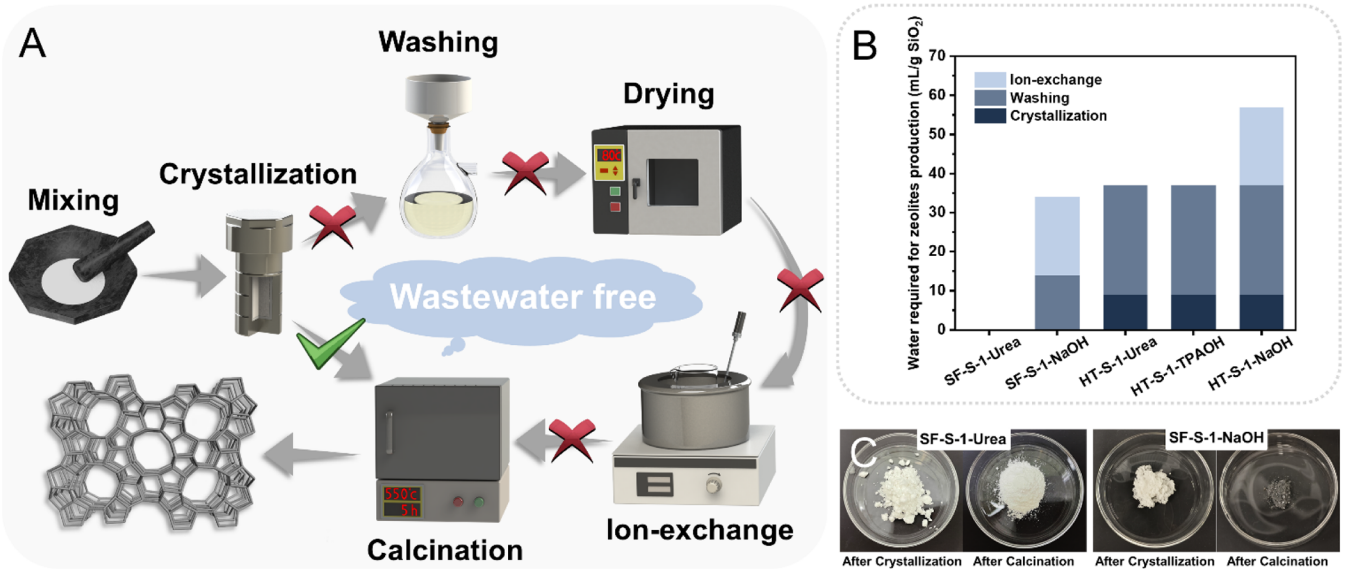

Figure 1. (A) Schematic representation of near-neutral and solvent-free synthesis. (B) Comparison of the consumed water for zeolite synthesis with urea, NaOH, and TPAOH in different routes. (C) Photos of the products of SF-S-1-Urea and SF-S-1-NaOH.

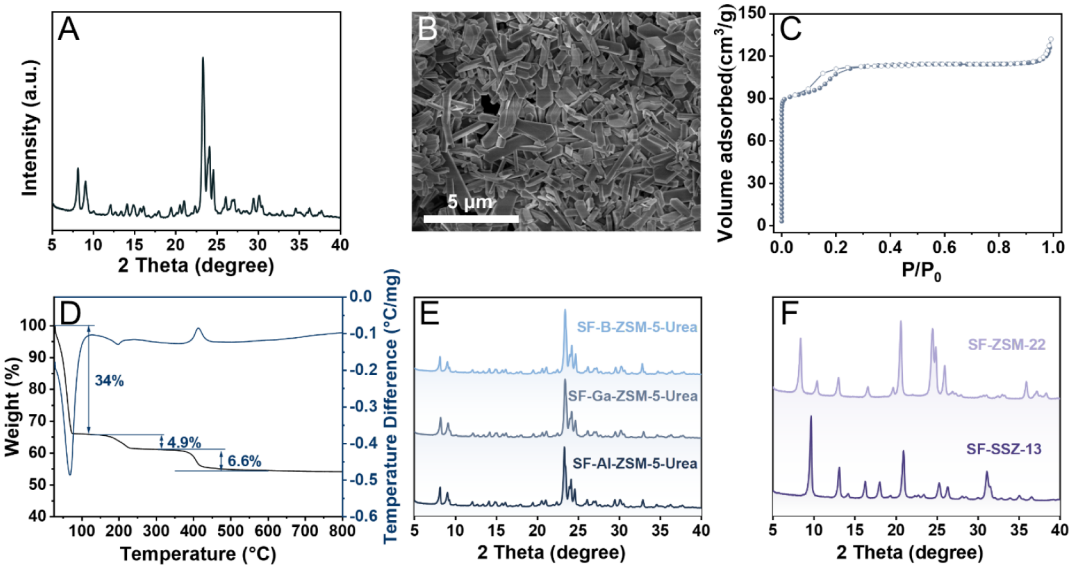

Figure 2. (A) XRD pattern, (B) SEM image, (C) N_2 sorption isotherms, and (D) TG-DTA curves of SF-S-1-Urea. (E) XRD patterns of SF-B-ZSM-5-Urea, SF-Ga-ZSM-5-Urea, and SF-Al-ZSM-5-Urea. (F) XRD patterns of SF-ZSM-22 and SF-SSZ-13.

RESULTS AND DISCUSSION

Figure 1A shows the scheme of the near-neutral and solvent-free synthesis of zeolites. In conventional synthesis, the procedures involve the mixing of raw materials, crystallization, washing, drying, ion exchange, and calcination, which are very complex and energy-consuming.[21−23] Meanwhile, the washing and ion-exchange steps are necessary, giving a large amount of wastewater. For the combination of near-neutral and solvent-free routes, there are almost no soluble silicate species or alkali metal cations in the urea-based synthetic system; therefore, it is not necessary to carry out the ion-exchange and water-washing steps. As a result, the zeolite synthesis can be simplified into three steps, including mixing, crystallization, and calcination.

Figure 1B compares water emissions during the synthesis of S-1 zeolites from various routes. Notably, the pure silica S-1 (MFI framework type) zeolite synthesized under near-neutral and solvent-free conditions in the presence of urea (SF-S-1-Urea) showed water-free emission. In contrast, the S-1 zeolite synthesized from a solvent-free route in the presence of NaOH (SF-S-1-NaOH) produced 34 mL of wastewater for each gram of SiO_2 due to water washing for the removal of alkali and soluble silicate species, as well as the ion-exchange of inorganic metal cations into protons. For the hydrothermal synthesis of S-1 zeolite, 9 mL of solvent water was required per gram of SiO_2.[24,25] For the synthesis of S-1 zeolites in the presence of urea (HT-S-1-Urea), TPAOH (HT-S-1-TPAOH), or NaOH (HT-S-1-NaOH), wastewater was generated at 37 mL, 37 mL, and 57 mL, respectively, because of washing and ion-exchange procedures. If the washing step for SF-S-1-NaOH was not performed, it would result in partial structural destruction during calcination, as shown by the dark gray sample for direct calcination (Figures S1 and 1C).[26,27] Therefore, the washing step cannot be avoided in the conventional synthesis of zeolites.

https://doi.org/10.1021/jacs.5c15625
J. Am. Chem. Soc. 2025, 147, 42901−42908

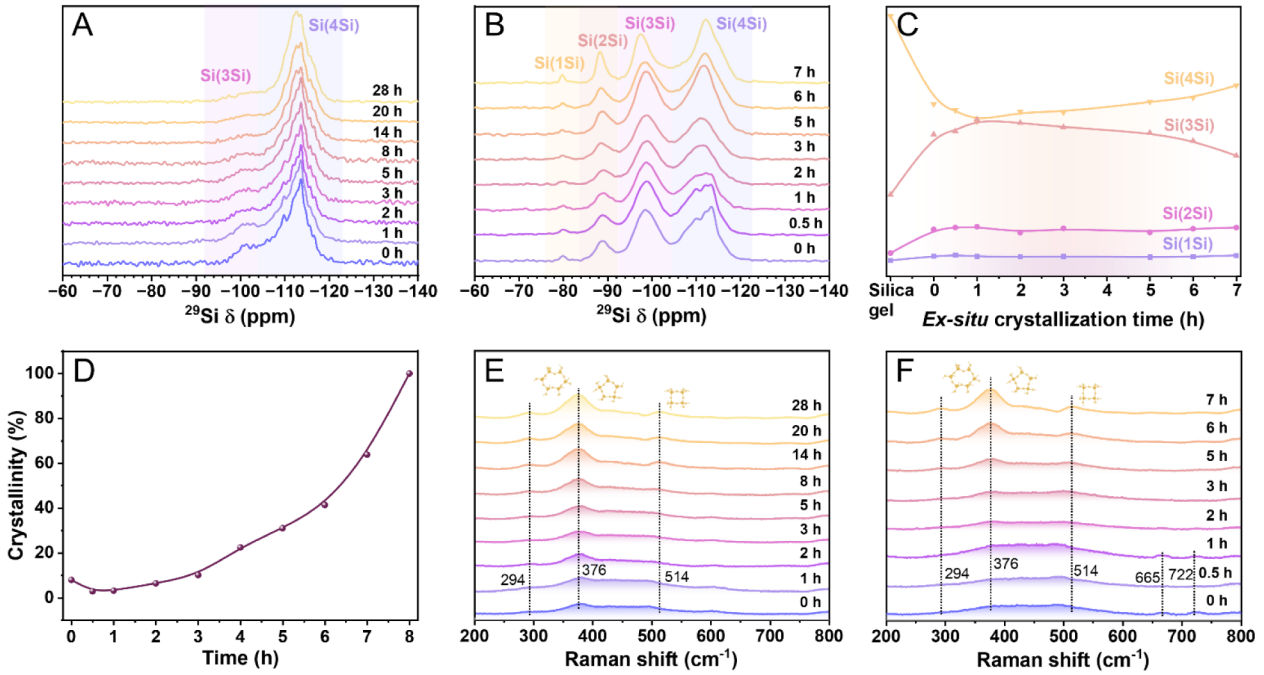

Figure 3. *Ex situ* ^{29}Si MAS NMR spectra of (A) SF-S-1-Urea and (B) SF-S-1-NaOH. (C) The changes in the coordination of Si species during the crystallization of SF-S-1-NaOH from quantitative analysis of peak area in the *ex situ* ^{29}Si MAS NMR spectra. (D) Crystallization curve of SF-S-1-NaOH. *Ex situ* UV Raman spectra of (E) SF-S-1-Urea and (F) SF-S-1-NaOH.

The solvent-free and near-neutral conditions not only minimize the dissolution of the silica source but also prevent the occupation of the volume within the autoclave by solvent, thereby enabling high yields and space-time yields. Furthermore, this work proposes a simplified synthesis process requiring only three steps to obtain the product, thereby avoiding the loss of the zeolite product related to the washing and ion exchange steps. It has been demonstrated that the yield of SF-S-1-Urea was 99.1%, which is significantly higher than the 86.8% and 84.3% yields of HT-S-1-TPAOH and HT-S-1-NaOH, respectively. The space-time yield of the novel method was 7.8 times that of HT-S-1-TPAOH and 8.1 times that of HT-S-1-NaOH under hydrothermal conditions. In addition, the feature of wastewater-free synthesis of zeolites also reduced the costs related to wastewater treatment. The cost for synthesis of SF-S-1-Urea was only 42% of HT-S-1-TPAOH and 59% of HT-S-1-NaOH.

X-ray diffraction (XRD) patterns of SF-S-1-Urea showed characteristic diffraction peaks related to the MFI structure (Figure 2A), in good agreement with the XRD pattern of the simulated structure (Figure S2). Scanning electron microscope (SEM) images of SF-S-1-Urea exhibited a typical morphology of MFI crystals (Figure 2B). N_2 sorption isotherms of SF-S-1-Urea gave a typical adsorption of type I isotherms with a Brunauer−Emmett−Teller (BET) surface area of 368 m^2/g (Figure 2C), which is comparable to those of MFI zeolites reported in the literature.[28,29] Thermogravimetric-differential thermal analysis (TG-DTA) curves of SF-S-1-Urea exhibited a major endothermic peak between room temperature and 120 °C due to the weight loss of physically adsorbed water. This finding suggests that during the initial calcination stage of SF-S-1-Urea, the majority of physically adsorbed water within the system can be effectively removed. Additionally, there was an endothermic peak from 120 to 300 °C related to chemically adsorbed water, followed by an exothermic peak from 300 to 600 °C, owing to the weight loss from TPA^+ decomposition (Figure 2D). In the TG curve of the as-made SF-S-1-Urea, there was no exothermic peak above 600 °C, indicating that the zeolite framework was stable. Furthermore, the calcined SF-S-1-Urea retained excellent crystallinity, confirming the excellent stability of the zeolite framework, as shown in Figure S3. In order to minimize gas emissions during calcination, the addition of an organic template and urea was optimized, giving minimum molar ratios of $TPACl/SiO_2$ and $Urea/SiO_2$ at 0.1, as presented in Table S1 and Figure S4. Moreover, TG analysis and elemental analysis of the as-made and calcined SF-S-1-Urea zeolites exhibited a weight loss of 6.6% between 300 and 600 °C, while the calcined sample showed a weight loss of less than 0.1% (Figure S5). The loss ranging from 300 to 600 °C was attributed to the organic template, and no loss over 600 °C was reasonably assigned to the stable zeolite framework. Furthermore, elemental analysis of SF-S-1-Urea revealed that there were no signals related to carbon and nitrogen, confirming the full elimination of TPA^+ species in the calcined zeolite (Table S2). In addition, Fourier transform infrared spectroscopy (FT-IR) spectra of the as-made and calcined SF-S-1-Urea zeolites were measured (Figure S6), and it was observed that the signals for C−H stretching vibrations around 3000 cm^{-1} and C−H bending vibrations near 1400 cm^{-1} entirely disappeared in the calcined SF-S-1-Urea zeolites, evidencing the effectiveness of the calcination.

Besides SF-S-1-Urea, a series of MFI zeolites containing heteroatoms (Al, B, and Ga), including SF-Al-ZSM-5-Urea, SF-B-ZSM-5-Urea, and SF-Ga-ZSM-5-Urea, were successfully synthesized under near-neutral and solvent-free conditions. The XRD patterns (Figure 2E), along with SEM images and magic angle spinning nuclear magnetic resonance (MAS NMR) spectra (Figure S7), demonstrate the synthesis of MFI topology zeolites with good crystallinity. Meanwhile, ^{27}Al, ^{11}B, and ^{71}Ga MAS NMR spectra indicate that heteroatoms were incorporated into the zeolite frameworks in tetrahedral coordination.[30−37] It has been reported that tetrahedrally coordinated Al at 51 to 59

https://doi.org/10.1021/jacs.5c15625
J. Am. Chem. Soc. 2025, 147, 42901−42908

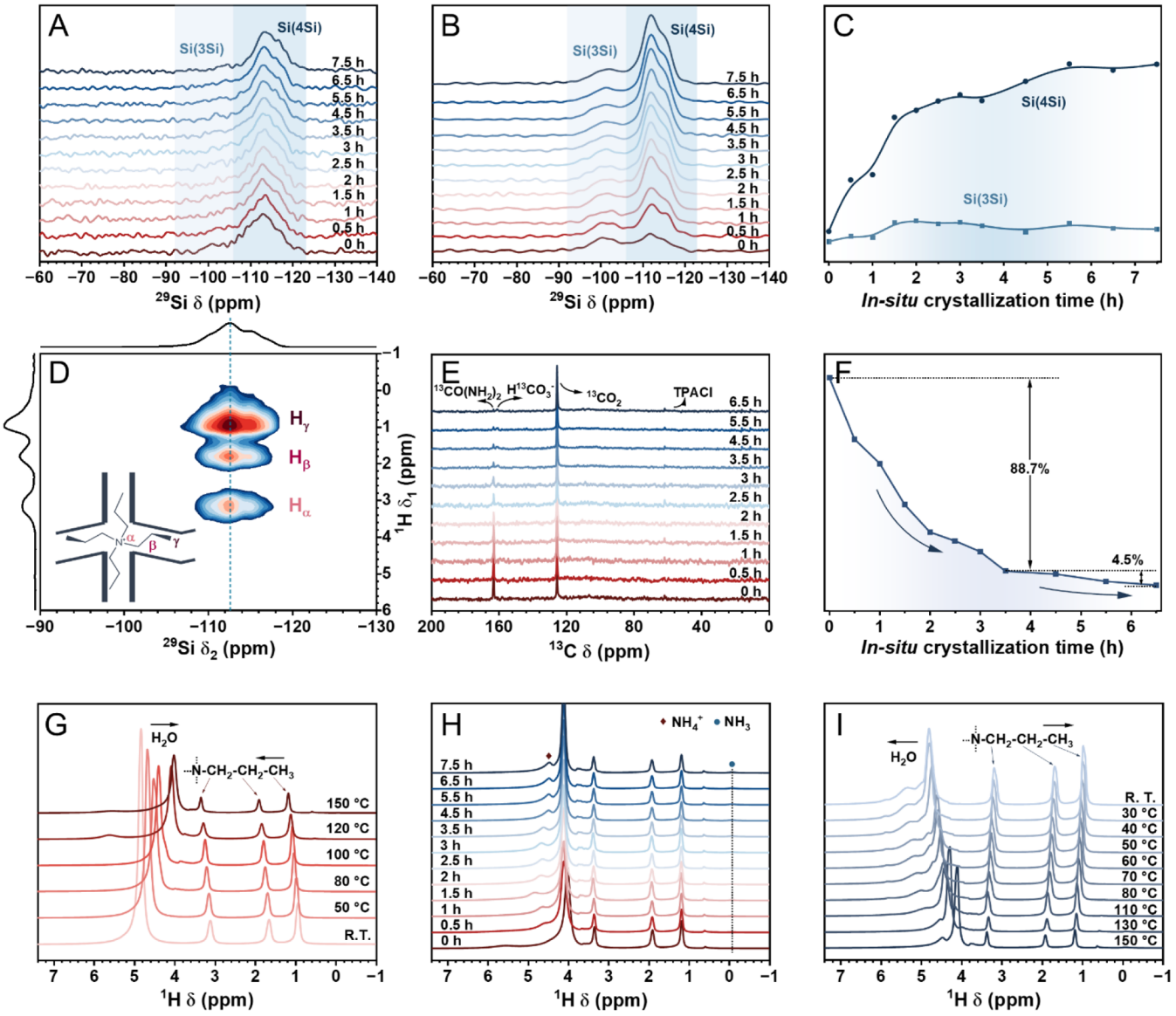

Figure 4. (A) *In situ* ^{29}Si MAS NMR spectra, (B) *in situ* ^{29}Si CP/MAS NMR spectra, (C) changes in the peak areas of Si(3Si) and Si(4Si) species during the crystallization process in the *in situ* ^{29}Si CP/MAS NMR spectra, (D) ^{1}H−^{29}Si FSLG-HETCOR MAS NMR spectra, (E) ^{13}C MAS NMR spectra, and (F) decomposition rate of urea during the crystallization of SF-S-1-Urea from quantitative analysis of the peak area of urea in the ^{13}C MAS NMR spectra. *In situ* ^{1}H MAS NMR of SF-S-1-Urea for (G) increasing temperature, (H) constant temperature, and (I) reducing temperature.

ppm, tetrahedrally coordinated B at −3.9 to −2.5 ppm, trigonally coordinated B at 0 to 15 ppm, and tetrahedrally coordinated Ga at 147 to 157 ppm in the zeolite frameworks, which are well consistent with those of ^{27}Al, ^{11}B, and ^{71}Ga MAS NMR spectra in this work (Figure S7), confirming that all of the heteroatoms have been incorporated into the zeolite frameworks.

Figure S3 shows XRD patterns and SEM images of calcined MFI zeolites. Notably, these zeolites retained their morphologies compared to the as-made zeolites. Inductively coupled plasma mass spectrometry (ICP-MS) analysis showed that the silicon-to-heteroatom molar ratios were unchanged before and after calcination, indicating that these heteroatoms in the zeolite frameworks are stable (Table S3). Beyond the MFI-type zeolite, CHA (SF-SSZ-13) and TON (SF-ZSM-22) topologies were also synthesized under near-neutral and solvent-free conditions, and their characteristic diffraction peaks and morphologies are shown in Figures 2F and S8. The N_2 sorption isotherms of SF-SSZ-13 and SF-ZSM-22 showed that the BET surface areas were 515 m^2/g and 115 m^2/g, respectively, which are comparable to those of samples synthesized by conventional hydrothermal synthesis.[38,39]

The utilization of urea in the synthesis of zeolites was usually performed at over 150 °C, which was related to the decomposition temperature of urea. Below 150 °C, the decomposition of urea was relatively weak. However, when urea was replaced with ammonia−water, S-1 zeolites with high crystallinity were still achieved even at temperatures of 100−140 °C (Figure S9). These findings demonstrate the general applicability of the proposed synthesis strategy.

Figure 3A exhibits the *ex situ* ^{29}Si MAS NMR spectra of SF-S-1-Urea. Prior to crystallization, the spectrum comprised a small proportion of Si(3Si) species and a dominant amount of Si(4Si) species, demonstrating that the majority of silica was in a highly condensed form.[40,41] As crystallization progressed, the content of Si(3Si) species gradually decreased, suggesting that the

https://doi.org/10.1021/jacs.5c15625
J. Am. Chem. Soc. 2025, 147, 42901−42908

amorphous silica had been rearranged during the crystallization process, which is consistent with the crystallization curve of SF-S-1-Urea (Figure S10). Figure 3B shows the *ex situ* ^{29}Si MAS NMR of SF-S-1-NaOH. Before the crystallization, the distribution of Si species included Si (1Si), Si(2Si), Si(3Si), and Si(4Si), suggesting substantial dissolution of silica under alkaline conditions. The evolution of silica species with crystallization time for SF-S-1-NaOH is illustrated in Figure 3C. The Si(3Si) increased within the first hour and then decreased slowly, while the Si(4Si) declined within the first hour and then gradually increased. These phenomena indicate that the hydrolysis of silica species proceeded more rapidly than condensation within the first hour. Subsequently, the condensation rate increased, leading to the gradual formation of the zeolite framework. This trend aligns well with the corresponding crystallization curves and XRD patterns (Figures 3D and S11). Figure 3E and F show the UV Raman spectra of SF-S-1-Urea and SF-S-1-NaOH. Both samples exhibited bands at 294, 376, and 514 cm^{-1}, which are related to S6R, S5R, and S4R species, respectively.[42] Notably, SF-S-1-NaOH exhibited additional bands at 665 cm^{-1} and 722 cm^{-1} attributed to the Si−OH species, which are well consistent with the presence of Si(1Si), Si(2Si), and Si(3Si) species in the *ex situ* ^{29}Si MAS NMR spectra of SF-S-1-NaOH.[43,44]

Compared with *ex situ* MAS NMR, *the in situ* MAS NMR technique can provide more detailed insights into zeolite crystallization under actual synthesis conditions.[45−48] However, *in situ* MAS NMR characterization of conventional hydrothermal synthesis of zeolite faces several challenges: (i) the high water content significantly increases the dielectric constant of the mixture, reducing detection efficiency; (ii) the solvent occupies space within the rotor, diminishing the signal-to-noise ratio; (iii) the presence of water limits the maximum achievable rotor spinning speed, thereby lowering spectral resolution; (iv) high autogenous pressure owing to additional water challenges the pressure resistance of rotors; and (v) the highly alkaline environment may corrode the ZrO_2 rotor, creating safety risks under high-temperature and high-pressure conditions. Furthermore, the low natural abundance of ^{29}Si and its long relaxation time present additional obstacles for *in situ* ^{29}Si NMR observation of zeolite crystallization.[49] In this study, zeolite crystallization was conducted under near-neutral and solvent-free conditions, effectively circumventing issues related to water solvent, high pressure, and rotor corrosion. Moreover, the use of ^{29}Si-enriched SiO_2 and ^{13}C-enriched urea significantly enhanced the sensitivity of *in situ* MAS NMR measurements, resulting in spectra with high signal-to-noise ratio.

Figure 4A shows the *in situ* ^{29}Si MAS NMR spectra of SF-S-1-Urea for a crystallization time of 7.5 h. This duration was selected owing to the good crystallinity of the S-1 zeolite within the *in situ* rotor at this point, as evidenced by the XRD pattern of the sample treated at 150 °C for 7.5 h (Figure S12). It is noteworthy that the Si(3Si) species decreased rapidly within the first hour of *in situ* crystallization, and thereafter, both Si(3Si) and Si(4Si) showed no significant changes. Moreover, Si(4Si) species remained dominant throughout the entire crystallization process from 0 to 7.5 h. These results indicate that crystallization primarily occurred via a solid-state phase transformation mechanism, consistent with findings from *ex situ* ^{29}Si MAS NMR spectroscopy. Figure 4B displays the corresponding ^{1}H→^{29}Si cross-polarization (CP) MAS NMR spectra, in which signals arise only from silicon atoms in close proximity to protons, such as those in Si−OH groups or the organic template. Interestingly, with increasing crystallization time, the Si(3Si) species remained basically unchanged, while the signals of the Si(4Si) species significantly increased. This is in contrast with both *ex situ* and *in situ* ^{29}Si MAS NMR results, suggesting that the enhancement in the peak intensity of the Si(4Si) species does not originate from the Si−OH species associated with Si(3Si) species (Figure 4C). To elucidate this phenomenon, ^{1}H−^{29}Si heteronuclear correlation experiments with Frequency Switched Lee Goldburg Heteronuclear Correlation (FSLG HETCOR) ^{1}H homonuclear decoupling were performed (Figure 4D).[50,51] The signals from both the methyl group at (−113, 1.0) and the two methylene groups at (−113, 1.7) and (−113, 3.2) of the template showed spatial proximity to the Si(4Si) species (at −113 ppm), while no significant cross-peaks between Si(4Si) and other hydrogen species, such as Si−OH, were observed. These results indicate that the signal enhancement at −113 ppm via cross-polarization in the *in situ* ^{29}Si CP/MAS NMR spectra (Figure 4B) during crystallization originates primarily from the TPA cations encapsulated within zeolite cavities, located at the junction of channels within MFI zeolites, rather than from the initial silica source or water (Figure S13). It is normally considered that the correlation between the framework Si−OH and Si(4Si) species is reasonable from the view of zeolite structure, but we cannot observe this interaction, which can be explained by three factors: (i) the low concentration of Si−OH species compared to that of H atoms in the template molecule, (ii) potential overlap with stronger methyl and methylene signals (isolated and hydrogen-bonded silanols at ca. 1.7−2.2 and 3−9 ppm in dehydrated S-1 zeolite, respectively), and (iii) the potential small transverse relaxation time ($T2$) value of ^{1}H spins in hydrogen-bonded silanols. In addition, the absence of a water signal can probably be attributed to its rapid motion. In conclusion, due to the dominance of the cross-peaks from methyl and methylene groups, it is safe to demonstrate the interaction between the template and the Si(4Si) species at −113 ppm.[52−55] Such an interaction may represent an important aspect of the templating effect exerted by TPA^+ cations in the synthesis of MFI zeolite.

Figure 4E shows *in situ* ^{13}C MAS NMR spectra of the SF-S-1-Urea under near-neutral and solvent-free conditions. Due to the use of ^{13}C-enriched urea, the signals corresponding to urea in the ^{13}C MAS NMR spectra were much stronger than those of TPACl. Under the applied conditions (150 °C), urea normally decomposes gradually to release CO_2. A portion of CO_2 dissolved, forming HCO_3^- species, indicating that the system was near-neutral. The peak area of urea in the ^{13}C MAS NMR spectra indicated that 88.4% of urea decomposed within the first 4 h at 150 °C, and only 4.5% of urea decomposed in the subsequent 2.5 h, suggesting that urea decomposition occurs predominantly during the early stages of the process (Figure 4F).

Figure 4G−I shows *in situ* ^{1}H MAS NMR spectra collected at various temperatures. During the heating stage (Figure 4G), the water signal at 4.9 ppm gradually shifted upfield, while the signal corresponding to TPA^+ shifted downfield. The upfield shift of the water peak is attributed to the breakdown of hydrogen bonds and an increased shielding effect, whereas the downfield shift of TPA^+ likely results from reduced solvent polarity and a deshielding environment. Throughout the isothermal stage at 150 °C (Figure 4H), a broad signal between 4 and 5 ppm is observed, which is potentially attributed to NH_4^+ produced by the dissolution of ammonia from the decomposition of urea.[56] After 1.5 h of thermal treatment, a new peak at −0.05 ppm

https://doi.org/10.1021/jacs.5c15625
J. Am. Chem. Soc. 2025, 147, 42901−42908

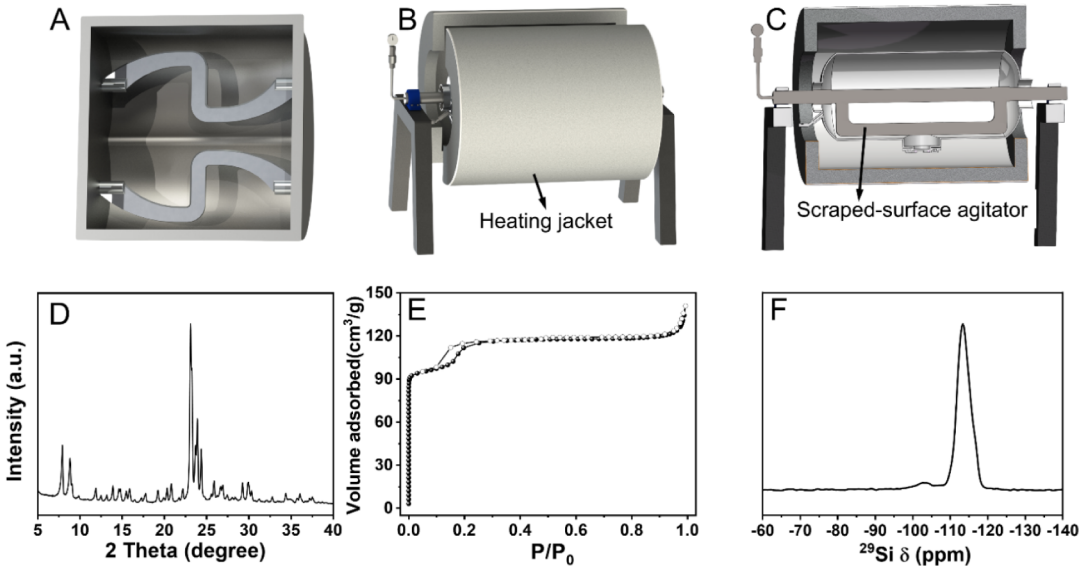

Figure 5. (A) Schematic representation of the mixer and (B and C) solid-state crystallizer. (D) XRD pattern, (E) N_2 sorption isotherms, and (F) ^{29}Si MAS NMR of SF-S-1-Urea-Scale-up synthesized in a 300 L reactor.

appeared, which is possibly assigned to excess ammonia following dissolution saturation.[57,58] The peak completely disappeared at 80 °C during the cooling stage (Figure 4I), consistent with the reversible dissolution of ammonia.

Furthermore, the route for the combination of near-neutral and solvent-free conditions can be scaled up from laboratory to industrial production. After mixing, crystallization, and calcination, the raw materials at a 150 kg scale were crystallized into zeolite products. The schematic diagram of the mixer is shown in Figure 5A. Moreover, a solid-state crystallizer with a capacity of 300 L has been designed for the industrial production of zeolites (SF-S-1-Urea-Scale-up, Figure 5B,C, Movies S1 and S2). The XRD pattern of the SF-S-1-Urea-Scale-up zeolite synthesized at 150 °C for 24 h showed good crystallinity (Figure 5D). In addition, the ^{29}Si MAS NMR spectrum of the product exhibited a large amount of Si(4Si) species with a small amount of Si(3Si) species, and the N_2 sorption isotherms of the product showed typical curves of micropores with a BET surface area of 389 m^2/g (Figure 5E,F). The SEM image of the SF-S-1-Urea-Scale-up zeolite exhibited perfect crystals without an amorphous phase (Figure S14). These results confirm the high quality of pure silica S-1 zeolite for industrial production.

To validate the performance of the products, we performed ^{29}Si MAS NMR and FT-IR spectra of SF-S-1-Urea, HT-S-1-TPAOH, and HT-S-1-NaOH. As shown in Figure S15, the peak area of the Si(3Si) species (framework defects Si−OH) in SF-S-1-Urea-Scale-up was 4.2%, which was lower than 5.0% and 6.9% for HT-S-1-NaOH and HT-S-1-TPAOH, respectively. These results suggest that the SF-S-1-Urea-Scale-up should have better hydrothermal and thermal stabilities than HT-S-1-NaOH and HT-S-1-TPAOH due to fewer defects of Si−OH. In addition, FT-IR spectra of the calcined zeolites showed that the SF-S-1-Urea-Scale-up had a much lower concentration of Si−OH with major nest silanols compared with HT-S-1-TPAOH and HT-S-1-NaOH, with major terminal and vicinal silanols, as shown in Figure S16. Because the silanol nests can easily condense to heal defects, it is reasonable that the SF-S-1-Urea-Scale-up is more stable than HT-S-1-TPAOH and HT-S-1-NaOH, which is critical for practical applications of zeolites in the future.

CONCLUSION

In summary, it has been demonstrated that a successful synthesis of silica-based zeolites, such as S-1, ZSM-5, ZSM-22, and SSZ-13, can be achieved under near-neutral and solvent-free conditions. Compared with conventional hydrothermal synthesis, the method in this work is very simple, containing only three steps: grinding, crystallization, and calcination, which represents a typical wastewater-free synthesis of zeolites. Very importantly, this zeolite synthesis can be scaled up to an industrial scale with a reactor of 300 L. Furthermore, *in situ* MAS NMR characterizations of S-1 zeolite reveal that the Si(4Si) species dominate throughout crystallization, consistent with a solid-state phase transformation mechanism. Particularly, the interaction between the methyl and methylene groups of TPA^+ and the Si(4Si) species in the framework was observed, which might be an important factor for the templating effect in zeolite crystallization.

EXPERIMENTAL SECTION

Synthesis of SF-S-1-Urea Zeolite. As a typical run, 1.9 g of $SiO_2 \cdot 3H_2O$, 0.185 g of TPACl, 0.1 g of urea, and 0.1 g of Silicalite-1 seed were added into the mortar. After grinding for 10 min, the homogeneous solid was transferred to an autoclave and heated at 150 °C for 24 h in an oven. After crystallization, the solid product was calcined at 550 °C for 5 h. The obtained product was denoted as SF-S-1-Urea.

ASSOCIATED CONTENT

Supporting Information

The Supporting Information is available free of charge at https://pubs.acs.org/doi/10.1021/jacs.5c15625.

Experimental details, materials, synthetic methods, and characterization details (PDF)

A mixer for the industrial production of zeolites (MP4)

A solid-state crystallizer with a capacity of 300 L has been designed for the industrial production of zeolites((MP4)

https://doi.org/10.1021/jacs.5c15625
J. Am. Chem. Soc. 2025, 147, 42901−42908

AUTHOR INFORMATION

Corresponding Authors

Qinming Wu − *Key Laboratory of Biomass Chemical Engineering of Ministry of Education and College of Chemical and Biological Engineering, Zhejiang University, Hangzhou 310028, China*; Email: qinmingwu@zju.edu.cn

Shutao Xu − *National Engineering Research Center of Lower-Carbon Catalysis Technology, Dalian Institute of Chemical Physics, Chinese Academy of Sciences, Dalian 116023, China*; orcid.org/0000-0003-4722-8371; Email: xushutao@dicp.ac.cn

Jihong Yu − *College of Chemistry, Jilin University, Changchun 130012, China*; orcid.org/0000-0003-1615-5034; Email: jihong@jlu.edu.cn

Feng-Shou Xiao − *Key Laboratory of Biomass Chemical Engineering of Ministry of Education and College of Chemical and Biological Engineering, Zhejiang University, Hangzhou 310028, China*; orcid.org/0000-0001-9744-3067; Email: fsxiao@zju.edu.cn

Authors

Lifan Deng − *Key Laboratory of Biomass Chemical Engineering of Ministry of Education and College of Chemical and Biological Engineering, Zhejiang University, Hangzhou 310028, China*

Caiyi Lou − *National Engineering Research Center of Lower-Carbon Catalysis Technology, Dalian Institute of Chemical Physics, Chinese Academy of Sciences, Dalian 116023, China; University of Chinese Academy of Sciences, Beijing 100049, China*; orcid.org/0000-0001-6204-0022

Xiaolong Liu − *School of Materials, Sun Yat-Sen University, Guangzhou 510275, China*; orcid.org/0000-0002-7346-7846

Jing Niu − *National Engineering Research Center of Lower-Carbon Catalysis Technology, Dalian Institute of Chemical Physics, Chinese Academy of Sciences, Dalian 116023, China*

Xiaohui Du − *Lanzhou Petrochemical Research Center, Petrochemical Research Institute, PetroChina, Lanzhou 730060, China*

Liang Wang − *Key Laboratory of Biomass Chemical Engineering of Ministry of Education and College of Chemical and Biological Engineering, Zhejiang University, Hangzhou 310028, China*; orcid.org/0000-0002-5826-1866

Zhongmin Liu − *National Engineering Research Center of Lower-Carbon Catalysis Technology, Dalian Institute of Chemical Physics, Chinese Academy of Sciences, Dalian 116023, China*; orcid.org/0000-0002-7999-2940

Complete contact information is available at: https://pubs.acs.org/10.1021/jacs.5c15625

Author Contributions

[▽]L.D. and C.L. contributed equally to this work.

Notes

The authors declare no competing financial interest.

ACKNOWLEDGMENTS

This work was supported by the National Natural Science Foundation of China (22288101, 22522208, U21B20101, 22172141, 22241801), the Dalian Outstanding Young Scientist Foundation (2021RJ01), the Liaoning International Joint Laboratory Project (2024JH2/102100005), the Zhejiang Provincial Natural Science Foundation of China under Grant No. LR24B030001, and the PetroChina Science and Technology Major Program (2023ZZ36).

REFERENCES

(1) Xu, R.; Pang, W.; Yu, J.; Huo, Q.; Chen, J. *Chemistry of Zeolite And Related Porous Materials* Wiley 2007.

(2) Mintova, S.; Olson, N. H.; Valtchev, V.; Bein, T. Mechanism of zeolite A nanocrystal growth from colloids at room temperature. *Science* **1999**, *283*, 958−960.

(3) Davis, M. E. Ordered porous materials for emerging applications. *Nature* **2002**, *417*, 813−821.

(4) Jeon, S.; Heo, T.; Hwang, S. Y.; Ciston, J.; Bustillo, K. C.; Reed, B. W.; Ham, J.; Kang, S.; Kim, S.; Lim, J.; et al. Reversible disorder-order transitions in atomic crystal nucleation. *Science* **2021**, *371*, 498−503.

(5) Breck, D. W. *Zeolite Molecular Sieves* Krieger 1984

(6) Li, Y.; Yu, J. Emerging applications of zeolites in catalysis, separation and host−guest assembly. *Nat. Rev. Mater.* **2021**, *6*, 1156−1174.

(7) Yang, J.; Huang, Y.-X.; Pan, Y.; Mi, J.-X. Green synthesis and characterization of zeolite silicalite-1 from recycled mother liquor. *Micropor. Mesopor. Mater.* **2020**, *303*, 110247.

(8) Sánchez-Hernández, R.; López-Delgado, A.; Padilla, I.; Galindo, R.; López-Andrés, S. One-step synthesis of NaP1, SOD and ANA from a hazardous aluminum solid waste. *Micropor. Mesopor. Mater.* **2016**, *226*, 267−277.

(9) Su, C.; Tian, S.; Li, K.; Dang, M.; Zhang, W.; Du, B.; Li, H.; Wang, L. *A method and system for treating wastewater in a molecular sieve production process* CN 114,477,653 B 2023.

(10) Xu, W.; Dong, J.; Li, J.; Li, J.; Wu, F. A novel method for the preparation of zeolites ZSM-5. *Chem. Commun.* **1990**, *10*, 755−756.

(11) Ren, L.; Wu, Q.; Yang, C.; Zhu, L.; Li, C.; Zhang, P.; Zhang, H.; Meng, X.; Xiao, F.-S. Solvent-free synthesis of zeolites from solid raw materials. *J. Am. Chem. Soc.* **2012**, *134*, 15173−15176.

(12) Meng, X.; Xiao, F.-S. Green routes for synthesis of zeolites. *Chem. Rev.* **2014**, *114*, 1521−1543.

(13) Deng, L.; Ma, Y.; Zai, T.; Yi, X.; Tong, Y.; Hui, Y.; Fan, K.; Wu, Q.; Ma, Y.; Liu, X.; Liu, W.; Sheng, N.; Wang, H.; Zheng, A.; Wang, L.; Xiao, F.-S. Atom-economic synthesis of zeolites. *J. Am. Chem. Soc.* **2024**, *146*, 29115−29122.

(14) Wu, D.; Yao, X.; Liang, L.; Deng, Q.; Han, L.; Hou, G.; Dai, W. Operando two-dimensional solid-state NMR unveils dual-template collaboration and competition in SAPO-34 zeolite crystallization. *J. Am. Chem. Soc.* **2025**, *147*, 18864−18875.

(15) Alahakoon, S. H.; Willans, M. J.; Huang, Y. *In situ* multinuclear magic-angle spinning NMR: monitoring crystallization of molecular sieve AlPO411 in real time. *JACS Au* **2023**, *3*, 1670−1683.

(16) Vistad, Ø. B.; Akporiaye, D. E.; Taulelle, F.; Lillerud, K. P. *In situ* NMR of SAPO-34 crystallization. *Anal. Chem.* **2003**, *15*, 1639−1649.

(17) Zhao, Z.; Xu, S.; Hu, M. Y.; Bao, X.; Hu, J. Z. *In situ* high temperature high pressure MAS NMR study on the crystallization of AlPO4−5. *J. Phys. Chem. C* **2016**, *120*, 1701−1708.

(18) Shi, J.; Anderson, M. W.; Carr, S. W. Direct observation of zeolite A synthesis by *in situ* solid-state NMR. *Chem. Mater.* **1996**, *8*, 369−375.

(19) Smaihi, M.; Barida, O.; Valtchev, V. Investigation of the crystallization stages of LTA-type zeolite by complementary characterization techniques. *Eur. J. Inorg. Chem.* **2003**, *2003*, 4370−4377.

(20) Ivanova, I. I.; Kolyagin, Y. G.; Kasyanov, I. A.; Yakimov, A. V.; Bok, T. O.; Zarubin, D. N. Time-resolved *in situ* MAS NMR monitoring of the nucleation and growth of zeolite BEA catalysts under hydrothermal conditions. *Angew. Chem., Int. Ed* **2017**, *56*, 15344−15347.

(21) Choi, M.; Na, K.; Kim, J.; Sakamoto, Y.; Terasaki, O.; Ryoo, R. Stable single-unit-cell nanosheets of zeolite MFI as active and long-lived catalysts. *Nature* **2009**, *461*, 246−249.

(22) Na, K.; Jo, C.; Kim, J.; Cho, K.; Jung, J.; Seo, Y.; Messinger, R. J.; Chmelka, B. F.; Ryoo, R. Directing zeolite structures into hierarchically nanoporous architectures. *Science* **2011**, *333*, 328−332.

(23) Yoo, W. C.; Kumar, S.; Penn, R. L.; Tsapatsis, M.; Stein, A. Growth patterns and shape development of zeolite nanocrystals in confined syntheses. *J. Am. Chem. Soc.* **2009**, *131*, 12377−12383.
(24) Pine, L. A.; Maher, P. J.; Wachter, W. A. Prediction of cracking catalyst behavior by a zeolite unit cell size model. *J. Catal.* **1984**, *85*, 466−476.
(25) Xu, M.; Liu, X.; Madon, R. J. Pathways for Y zeolite destruction: The role of sodium effect on USY zeolite. *J. Catal.* **2011**, *393*, 171−177.
(26) Du, X.; Li, X.; Zhang, H.; Gao, X. Kinetics study and analysis of zeolite Y destruction. *J. Catal.* **2016**, *37*, 316−323.
(27) Xie, L.; Liu, F.; Shi, X.; Xiao, F.-S.; He, H. Effects of post-treatment method and Na co-cation on the hydrothermal stability of Cu−SSZ-13 catalyst for the selective catalytic reduction of NO_x with NH_3. *Appl. Catal., B* **2015**, *179*, 206−212.
(28) Wu, Q.; Zhu, L.; Chu, Y.; Liu, X.; Zhang, C.; Zhang, J.; Xu, H.; Xu, J.; Deng, F.; Feng, Z.; Meng, X.; Xiao, F.-S. Sustainable synthesis of pure silica zeolites from a combined strategy of zeolite seeding and alcohol filling. *Angew. Chem., Int. Ed* **2019**, *58*, 12138−12142.
(29) Karim, T. M.; Toyoda, H.; Sawada, M.; Zhao, L.; Wang, Y.; Xiao, P.; Wang, L.; Huang, J.; Yokoi, T. Aluminum distribution on the microporous and hierarchical ZSM-5 intracrystalline and its impact on the catalytic performance. *Chem. Bio. Eng.* **2024**, *1*, 805−816.
(30) Zhou, H.; Yi, X.; Hui, Y.; Wang, L.; Chen, W.; Qin, Y.; Wang, M.; Ma, J.; Chu, X.; Wang, Y.; Hong, X.; Chen, Z.; Meng, X.; Wang, H.; Zhu, Q.; Song, L.; Zheng, A.; Xiao, F.-S. Isolated boron in zeolite for oxidative dehydrogenation of propane. *Science* **2021**, *372*, 76−80.
(31) Liang, T.; Chen, J.; Qin, Z.; Li, J.; Wang, P.; Wang, S.; Wang, G.; Dong, M.; Fan, W.; Wang, J. Conversion of methanol to olefins over H-ZSM-5 zeolite: reaction pathway is related to the framework aluminum siting. *ACS Catal.* **2016**, *6*, 7311−7325.
(32) Nigro, E.; Crea, F.; Testa, F.; Aiello, R.; Lentz, P.; Nagy, J. B. The role of alkali cations in the synthesis of Ga-ZSM-5 in fluoride medium. *Micropor. Mesopor. Mater.* **1999**, *30*, 199−211.
(33) Gao, P.; Xu, J.; Qi, G.; Wang, C.; Wang, Q.; Zhao, Y.; Zhang, Y.; Feng, N.; Zhao, X.; Li, J.; Deng, F. A mechanistic study of methanol-to-aromatics reaction over Ga-modified ZSM-5 zeolites: understanding the dehydrogenation process. *ACS Catal.* **2018**, *8*, 9809−9820.
(34) Massiot, D.; Vosegaard, T.; Magneron, N.; Trumeau, D.; Montouillout, V.; Berthet, P.; Loiseau, T.; Bujoli, B. ^{71}Ga NMR of reference Ga_{IV}, Ga_V, and Ga_{VI} compounds by MAS and QPASS, extension of gallium/aluminum NMR parameter correlation. *Solid State Nucl. Magn. Reson.* **1999**, *15*, 159−169.
(35) Ma, D.; Shu, Y.; Zhang, C.; Zhang, W.; Han, X.; Xu, Y.; Bao, X. Synthesis and characterization of galloaluminosilicate/gallosilicalite (MFI) and their evaluation in methane dehydro-aromatization. *J. Mol. Catal. A: Chem.* **2001**, *168*, 139−146.
(36) Crosson, G. S.; Choi, S.; Chorover, J.; Amistadi, M. K.; O'Day, P. A.; Mueller, K. T. Solid-state NMR identification and quantification of newly formed aluminosilicate phases in weathered kaolinite systems. *J. Phys. Chem. B* **2006**, *110*, 723−732.
(37) Yakimov, A. V.; Ravi, M.; Verel, R.; Sushkevich, V. L.; van Bokhoven, J. A.; Coperet, C. Structure and framework association of lewis acid sites in MOR zeolite. *J. Am. Chem. Soc.* **2022**, *144*, 10377−10385.
(38) Shan, Y.; Shan, W.; Shi, X.; Du, J.; Yu, Y.; He, H. A comparative study of the activity and hydrothermal stability of Al-rich Cu-SSZ-39 and Cu-SSZ-13. *Appl. Catal., B* **2020**, *264*, 118511.
(39) Mallette, A. J.; Shilpa, K.; Rimer, J. D. The current understanding of mechanistic pathways in zeolite crystallization. *Chem. Rev.* **2024**, *124*, 3416−3493.
(40) White, J. R.; Cameron, A. E. The natural abundance of isotopes of stable elements. *Phys. Rev.* **1948**, *74*, 991−1000.
(41) Brouwer, D. Applications of Silicon-29 NMR spectroscopy In *Reference Module in Chemistry, Molecular Sciences and Chemical Engineering* Elsevier 2021.
(42) Wu, Q.; Wang, X.; Qi, G.; Guo, Q.; Pan, S.; Meng, X.; Xu, J.; Deng, F.; Fan, F.; Feng, Z.; Li, C.; Maurer, S.; Müller, U.; Xiao, F.-S. Sustainable synthesis of zeolites without addition of both organo-templates and solvents. *J. Am. Chem. Soc.* **2014**, *136*, 4019−4025.
(43) Zhang, L.; Chen, K.; Chen, B.; White, J.; Resasco, D. E. Factors that determine zeolite stability in hot liquid water. *J. Am. Chem. Soc.* **2015**, *137*, 11810−11819.
(44) Zhang, J.; Chu, Y.; Liu, X.; Xu, H.; Meng, X.; Feng, Z.; Xiao, F.-S. Interzeolite transformation from FAU to CHA and MFI zeolites monitored by UV Raman spectroscopy. *J. Catal.* **2019**, *40*, 1854−1859.
(45) Shi, X.; Lin, X.; Luo, R.; Wu, S.; Li, L.; Zhao, Z.; Gong, J. Dynamics of heterogeneous catalytic processes at operando conditions. *JACS Au* **2021**, *1*, 2100−2120.
(46) Weckhuysen, B. M. Snapshots of a working catalyst: possibilities and limitations of in situ spectroscopy in the field of heterogeneous catalysis. *Chem. Commun.* **2002**, 97−110.
(47) Weckhuysen, B. M. Determining the active site in a catalytic process: Operando spectroscopy is more than a buzzword. *Phys. Chem. Chem. Phys.* **2003**, *5*, 4351−4360.
(48) Bañares, M. A. Operando methodology: combination of in situ spectroscopy and simultaneous activity measurements under catalytic reaction conditions. *Catal. Today* **2005**, *100*, 71−77.
(49) Liu, X.; Luo, Q. Solid State NMR Spectroscopy studies of the nature of structure direction of OSDAs in pure-silica zeolites ZSM-5 and Beta. *J. Phys. Chem. C* **2017**, *121*, 13211−13217.
(50) van Rossum, B. J.; Förster, H.; de Groot, H. J. M. High-field and high-speed CP-MAS ^{13}C NMR heteronuclear dipolar-correlation spectroscopy of solids with frequency-switched Lee-Goldburg homonuclear decoupling. *Magn. Reson.* **1997**, *124*, 516−519.
(51) Lesage, A.; Emsley, L. Through-bond heteronuclear single-quantum correlation spectroscopy in solid-state NMR, and comparison to other through-bond and through-space experiments. *J. Magn. Reson.* **2001**, *148*, 449−454.
(52) Chen, L.; Lu, P.; Yuan, Y.; Xu, L.; Zhang, X.; Xu, L. Hydrothermal synthesis of nanosized ZSM-22 and their use in the catalytic conversion of methanol. *J. Catal.* **2016**, *37*, 1381−1388.
(53) Liu, C.; Qi, G.; Gong, Y.; Wang, D.; Fu, W.; Liu, F.; Xu, J.; Liu, D.; Wang, Z.; Yang, W. Modulation of Al sites in MWW zeolites with enhanced catalytic performance by dual organic structure-directing agents. *Chem. Bio. Eng.* **2025**, *2*, 358−369.
(54) Paul, G.; Bisio, C.; Braschi, I.; Cossi, M.; Gatti, G.; Gianotti, E.; Marchese, L. Combined solid-state NMR, FT-IR and computational studies on layered and porous materials. *Chem. Soc. Rev.* **2018**, *47*, 5684−5739.
(55) Luo, Q.; Yang, J.; Hu, W.; Zhang, M.; Yue, Y.; Ye, C.; Deng, F. Unambiguously distinguishing Si[3Si,1Al] and Si[3Si,1OH] structural units in zeolite by ^{1}H/^{29}Si/^{27}Al triple resonance solid state NMR spectroscopy. *Solid State Nucl. Magn. Reson.* **2005**, *28*, 9−12.
(56) Buchholz, A.; Wang, W.; Xu, M.; Arnold, A.; Hunger, M. Sequential steps of ammoniation of the microporous silicoaluminophosphates H-SAPO-34 and H-SAPO-37 investigated by *in situ* CF MAS NMR spectroscopy. *J. Phys. Chem. B* **2004**, *108*, 3107−3113.
(57) Jacobs, W. P. J. H.; de Haan, J. W.; van de Ven, L. J. M.; van Santen, R. A. Interaction of ammonia with Bronsted acid sites in different cages of zeolite Y as studied by proton MAS NMR. *J. Phys. Chem.* **1993**, *97*, 10394−10402.
(58) Ernst, H.; Freude, D.; Hunger, M.; Pfeifer, H.; Seiffert, B. High-resolution H^1 nuclear-magnetic-resonance of various aluminosilicate catalysts treated with ammonia. *Z. Phys. Chem.* **1987**, *268*, 304−314.

https://doi.org/10.1021/jacs.5c15625
J. Am. Chem. Soc. 2025, 147, 42901−42908